FULL PAPER

Charge Photogeneration for a Series of Thiazolo-Thiazole Donor Polymers Blended with the Fullerene Electron Acceptors PCBM and ICBA

Safa Shoaee, Selvam Subramaniyan, Hao Xin, Chaz Keiderling, Pabitra Shakya Tuladhar, Fiona Jamieson, Samson A. Jenekhe, and James R. Durrant**

Photoinduced charge separation in bulk heterojunction solar cells is studied using a series of thiazolo-thiazole donor polymers that differ in their side groups (and bridging atoms) blended with two acceptor fullerenes, phenyl-C_{71}-butyric acid methyl ester ($PC_{71}BM$) and a fullerene indene-C60 bisadduct (ICBA). Transient absorption spectroscopy is used to determine the yields and lifetimes of photogenerated charge carriers, complimented by cyclic voltammetry studies of materials energetics, wide angle X-ray diffraction and transmission electron microscopy studies of neat and blend film crystallinity and photoluminescence quenching studies of polymer/fullerene phase segregation, and the correlation of these measurements with device photocurrents. Good correlation between the initial polaron yield and the energetic driving force driving charge separation, ΔE_{CS} is observed. All blend films exhibit a power law transient absorption decay phase assigned to non-geminate recombination of dissociated charges; the amplitude of this power law decay phase shows excellent correlation with photocurrent density in the devices. Furthermore, for films of one (relatively amorphous) donor polymer blended with ICBA, we observe an additional 100 ns geminate recombination phase. The implications of the observations reported are discussed in terms of the role of materials' crystallinity in influencing charge dissociation in such devices, and thus materials design requirements for efficient solar cell function.

1. Introduction

Bulk heterojunction (BHJ) organic solar cells[1] based on blend films of electron donating polymers with electron accepting fullerenes are receiving extensive academic and commercial interest. One of the key challenges for the development of such solar cells is the identification of the key materials properties that determine photovoltaic device performance. In this regard, increasing attention is being placed on analyses of the microstructure of such blend films, and how this impacts upon device performance.[2–5] It is becoming apparent that simple structural models of such polymer/fullerene blend films as comprising bicontinuous, interpenetrating donor and acceptor domains are inadequate to explain photovoltaic function, with attention increasingly focused upon the presence of mixed donor/acceptor domains[5–8] and variations in materials crystallinity[9,10] both within a single film and between materials. In this study we address these issues by a systematic study of how a variation in molecular structure, and thereby film microstructure and energetics, can vary the efficiency of photoinduced charge separation, and thereby the efficiency of photocurrent generation, in such BHJ solar cells.

The materials considered in this study comprise a series of thiazolothiazole-based donor polymers blended with two different fullerene acceptors. The polymers varied only in their alkyl side group composition, which in turn varied both the energetics and crystallinity of these donor polymers. For acceptors, we employed the widely used fullerene phenyl-C_{71}-butyric acid methyl ester ($PC_{71}BM$), as well as the fullerene indene-C60 bisadduct ICBA.[11] ICBA has been previously shown, when blended with poly(3-hexylthiophene) (P3HT), to result in a higher device voltage than PCBM due to its smaller electron affinity, and thus enhanced device performance.[11] The chemical structures of these materials are shown in **Scheme 1**. We have previously reported BHJ device performance data for some of this materials series.[12] In particular, we have observed that several, but not all, of the donor polymers exhibit promising device photocurrents in blends with both ICBA and PCBM. This is of particular interest as ICBA has more typically been found to give relatively poor photocurrents when blended with alternative donor polymers to P3HT.[13] We address this issue here, focusing upon the quantitative correlations between material crystallinity and energetics with the yield and lifetimes

Dr. S. Shoaee, C. Keiderling, Dr. P. S. Tuladhar, Dr. F. Jamieson, Prof. J. R. Durrant
Centre for Plastic Electronics and Department of Chemistry
Imperial College London, London SW7 2AZ, UK
E-mail: s.shoaee06@imperial.ac.uk; j.durrant@imperial.ac.uk
Dr. S. Subramaniyan, Dr. H. Xin, Prof. S. A. Jenekhe
Department of Chemical Engineering
University of Washington
Seattle, Washington 98195-1750, USA

DOI: 10.1002/adfm.201203148

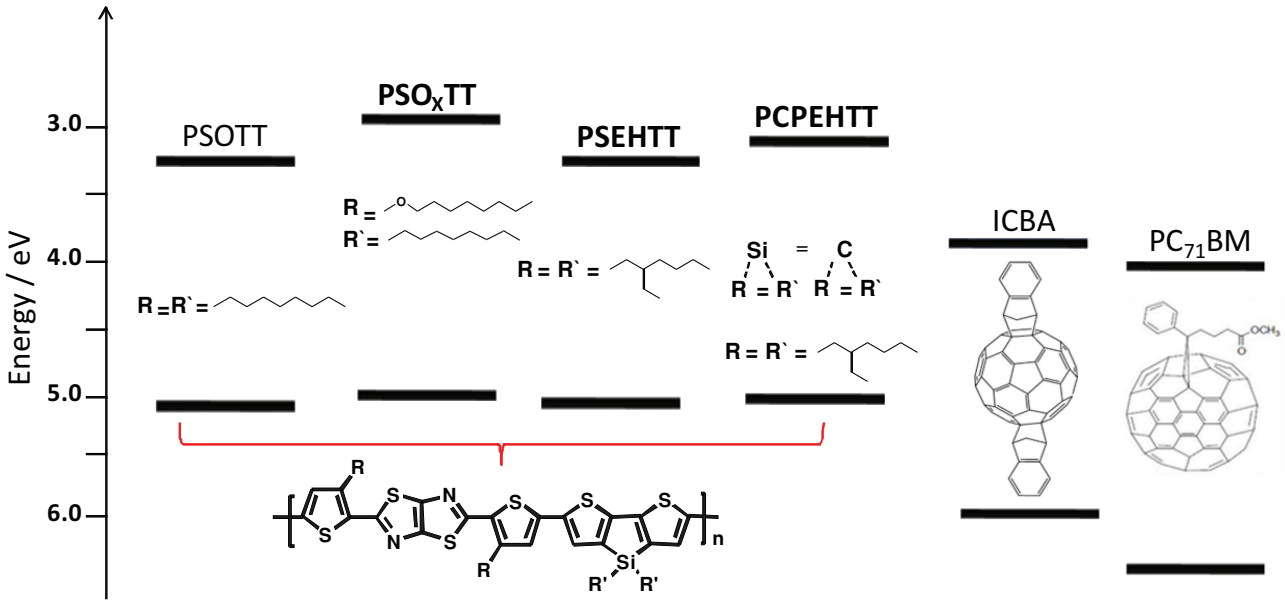

Scheme 1. Structures of the donor polymers and acceptor fullerenes studied herein, material ionization potentials (IP) determined by cyclic voltammetry of neat films, and material electron affinities determined from these IP data combined with optical bandgaps, taken from previous references.[17,18]

of photogenerated charge carriers, and thereby photocurrent density. We consider in particular the dependence of geminate recombination of photogenerated charges upon not only energetics but also materials structure; geminate recombination being widely proposed as a key factor determining the efficiency of photocurrent generation in many bulk heterojunction devices.[14–16]

Significant progress has been made in relating the voltage output of organic solar cells to material properties, specifically to the energy difference between the donor ionization potential and acceptor electron affinity.[19–21] However, beyond simple correlations with material bandgap, and thereby solar light harvesting efficiency, progress in predicting device photocurrent densities on the basis of materials or film properties has proved much more problematic. We and others have previously shown that, for some materials series, correlations can be observed between the energy offset driving charge separation, the yield of dissociated charge carriers and device photocurrent densities.[22–24] However it is also apparent that other factors may also be important.[13,25,26] Of particular relevance to the study herein, it has been widely shown that material crystallinity impacts directly upon the BHJ film microstructure, charge carrier mobility[27] and materials energetics, with increased crystallinity typically reducing the electrical and/or optical bandgaps of the material.[10,28,29] Previous studies of the effect of thermal annealing on P3HT:PC$_{60}$BM have reported correlations between materials crystallinity, geminate recombination losses and short circuit photocurrent in devices.[30,31] In addition, several recent studies have emphasized the miscibility of PCBM with donor polymers, resulting in the formation of relatively amorphous, intimately mixed donor/acceptor domains,[8,32–34] with this miscibility being dependent upon polymer crystallinity.[6,8,35,36] It has also been reported that this miscibility (or intercalation) of acceptor fullerenes with donor polymers can be different with bis- rather than mono- adducts, with this impacting significantly upon device performance.[37] In this regard, we have recently provided evidence that the tendency of PC$_{60}$BM to form aggregated, relatively pure PC$_{60}$BM domains alongside a mixed phase, with these aggregated PC$_{60}$BM domains exhibiting a higher electron affinity, may be a key factor behind the ubiquitous success of PC$_{60}$BM as an acceptor in BHJ devices.[10] In this paper, we explore this characteristic of PCBM further, in particular with regard to materials design criteria for both donors and acceptors in bulk heterojunction solar cells.

2. Results

The structures of the series of thiazolo-thiazole donor polymers employed in this study, which differ in their side groups (and bridging atoms), are shown in Scheme 1, alongside the two fullerene acceptors PC$_{71}$BM and ICBA. The synthesis and limited functional evaluation of these polymers have been reported elsewhere.[12,17,18] Also show in Scheme 1 are approximate values for the materials highest occupied molecular orbital (HOMO) and lowest unoccupied molecular orbital (LUMO) energies by cyclic voltammetry (CV) of films (for polymers) and solutions (for fullerenes), as reported previously.[11,17] It is apparent from these energy levels that for all of the blend films studied, there should be an significant LUMO level offset between the donor polymers and acceptor fullerenes (ranging between 0.41 and 0.67 eV) to drive photoinduced electron transfer. We note however that these HOMO and LUMO levels were not determined for blend films but for neat films or solutions, as is typical in the literature; we discuss below the variation of these energy levels with blend formation.

Photovoltaic device performance of most of the blend films addressed herein have been reported previously, with

Table 1. Summary of data obtained for the blend films studied here, including photoluminescence quenching, materials crystallinity determined from XRD data, polaron yields determined from transient absorption data, device photocurrent densities, and estimates of the energy difference driving charge separation determined from blend film data.

Blend	[a]PLQ	Crystallinity in the blend: Polymer	Crystallinity in the blend: fullerene	[b]ΔOD	J_{SC} (Acm^{-2})	[d]ΔE_{CS}^{eff} (eV)
PSEHTT:PCBM	0.88	✓	✓	9.5×10^{-5}	10.7×10^{-3}	0.53
PSEHTT:ICBA	0.93	✓	✓	1.1×10^{-4}	11.0×10^{-3}	0.51
PSOTT:PCBM	0.90	✓	✓	8.0×10^{-5}	9.8×10^{-3}	0.49
PSOTT:ICBA	0.92	✓	✓	4.0×10^{-5}	6.2×10^{-3}	0.47
PSO_XTT:PCBM	0.90	✓	✓	3.6×10^{-5}	6.7×10^{-3}	0.43
PSO_XTT:ICBA	0.92	✓	✓	2.5×10^{-5}	4.6×10^{-3}	0.41
PCPEHTT:PCBM	0.99	✗	✓	3.0×10^{-5}	5.1×10^{-3}	0.43
PCPEHTT:ICBA	0.99	✗	✗	2.0×10^{-5c} 3.5×10^{-6}	1.5×10^{-3}	0.41

[a]Steady-state PL quenching of the blend film relative to the corresponding pristine polymer film; [b]initial amplitude (determined at 20 ns, at 3 μJ cm^{-2} of the Δ*OD* signal assigned to polaron absorption, after correction for the ground state absorbance at the excitation wavelength; [c]as for b except determined from extrapolation of the power-law decay phase back to 20 ns; [d]ΔE_{CS}^{eff} estimated from E_S - (IP - EA), where E_S the singlet exciton energy of the donor, measured from mid-point of the polymer absorption and emission spectra in the blend film, IP is the polymer ionization potential and EA is the fullerene electron affinity, determined from values of IP and EA measured from cyclic voltammetry of 1:1 blend films (see Supporting Information for details).

poly[(4,4′-bis(3-(2-ethyl-hexyl)dithieno[3,2-b:″,3′-d]silole)-2,6-diyl-alt-(2,5-bis(3-(2-ethyl-hexyl)thiophen-2yl)thiazolo[5,4-d]thiazole)] PSEHTT:ICBA blend films yielding device efficiencies in excess of 5%.[12] Current–voltage (*J*–*V*) curves for Poly[(4,4′-bis(3-(2-ethyl-hexyl)-4H-cyclopenta[2,1-b;3,4-b′]dithiophene)-2,6-diyl-alt-(2,5-bis(3-(2-ethyl-hexyl)thiophen-2yl)thiazolo[5,4-d] thiazole)] (PCPEHTT) devices are shown in supporting information, the analogous data for other donor polymers has been reported previously.[12] Herein we focus only upon photocurrent generation, with short circuit photocurrents J_{SC} obtained for all blend films studied listed in **Table 1**. This paper is concerned with a quantitative understanding of the origin of the observed variation in photocurrent densities, which range from 1.5 to 11.2 mA cm^{-2}.

2.1. Material Crystallinity and Energetics

We first consider the relative crystallinities of the materials studied. Wide angle X-ray diffraction (XRD) was employed as a qualitative assay of relative crystallinity of these materials as neat and blend drop cast films. We note that the use of drop cast films results in relatively random material orientation, simplifying analyses of these XRD data. Typical XRD data for representative films are shown in **Figure 1**. It can be concluded that neat Poly[(4,4′-bis(2-octyl)dithieno[3,2-b:″,3′-d]silole)-2,6-diyl-alt-(2,5-bis(3-octylthiophen-2yl)thiazolo[5,4-d]thiazole)] (PSOTT) films are highly crystalline, with crystallinity comparable to that of P3HT. In contrast neat films of PCPEHTT show much lower crystallinity. This difference in crystallinity is even more pronounced in blend films with $PC_{71}BM$ or ICBA, with either fullerene only having a modest impact on the crystallinity of P3HT and PSOTT, but almost completely removing the (already weaker) polymer XRD peak for PCPEHTT. Analogous XRD data were obtained for all the neat and blend films studied here and are summarized in Table 1.

Further evidence for differences in the crystallinity of the polymer in the blend films was obtained from transmission electron microscopy (TEM), as shown in **Figure 2**. TEM images for PSOTT:$PC_{71}BM$ blend films show clear evidence of phase segregation on the tens of nanometres length scale. Furthermore high magnification micrographs of these films (Figure 2) shows clear evidence for the crystallinity and chemical purity of the PSOTT domains, exhibiting clear diffraction fringes corresponding to the lattice spacing of the PSOTT crystallites (≈2 nm), in agreement with the XRD data and typical of that observed for PSOTT crystallites.[17] In contrast to PSOTT, TEM studies of PCPEHTT blend films showed no evidence of such long length scale phase segregation (see Supporting Information), nor the presence of diffraction fringes, consistent with these films being relatively amorphous, in agreement with our XRD data. It should be noted that our observation of lattice fringes for PSOTT:$PC_{71}BM$ films is clear evidence of the high crystallinity of this polymer; to the best of our knowledge such TEM lattice fringes in BHJ organic photovoltaic (OPV) blend films have only previously been reported for P3HT in P3HT:$PC_{60}BM$ blend films.[38]

Additional data on the impact of blending with fullerene upon polymer crystallinity was obtained by film CV data. A decrease in material crystallinity typically results in an increased

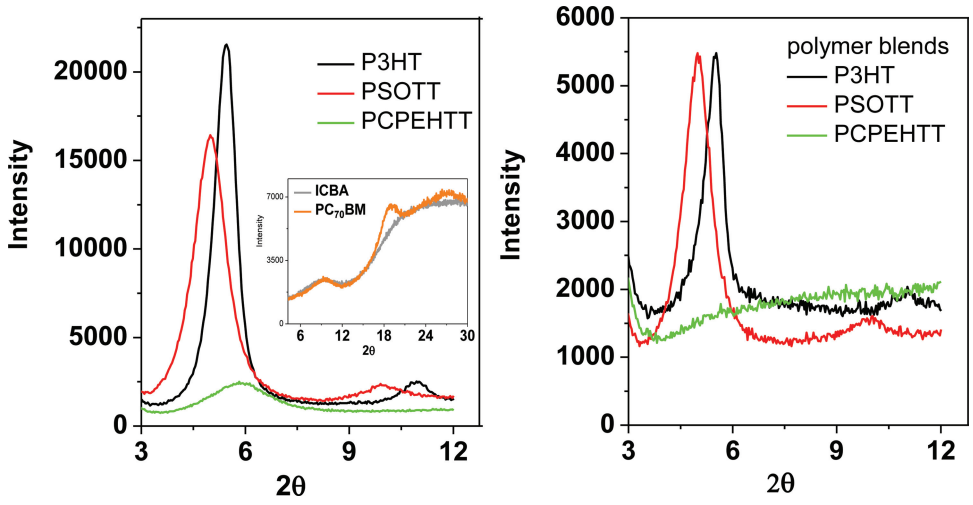

Figure 1. Wide-angle X-ray diffractograms of PSOTT, PCPEHTT and P3HT drop cast neat films (left) and 1:1 blend films with $PC_{71}BM$ (right), showing PSOTT exhibits similar crystallinity to P3HT, whilst PCPEHTT only exhibit weak X-ray diffraction in neat film, and almost no diffraction in blend film with fullerene, and is therefore relatively amorphous. Analogous data were obtained for all polymers studied, in blends with both PCBM and ICBA; the results are summarized in Table 1. The inset of the left plot displays XRD spectra of neat ICBA and $PC_{71}BM$ films, showing enhanced X-ray diffraction for PCBM relative to ICBA.

electronic bandgap,[28,29] as for example we have previously reported for P3HT, where annealing of blend films resulted in an increase in P3HT crystallinity and a corresponding decrease of its ionization potential.[39] For the crystalline polymer PSOTT, no shift in its oxidation wave was observed between neat and blend films (to within ±25 mV), consistent with the invariance of the XRD data, and indicating that blending with fullerene does not significantly disrupt the materials crystallinity. In contrast, for the more amorphous polymer PCPEHTT, a shift was observed in its oxidation wave by 150–200 mV between neat films and 1:1 blends with either $PC_{71}BM$ or ICBA, consistent with the XRD data which indicates that for this polymer, addition of either fullerene reduces the (already limited) crystallinity of the polymer.

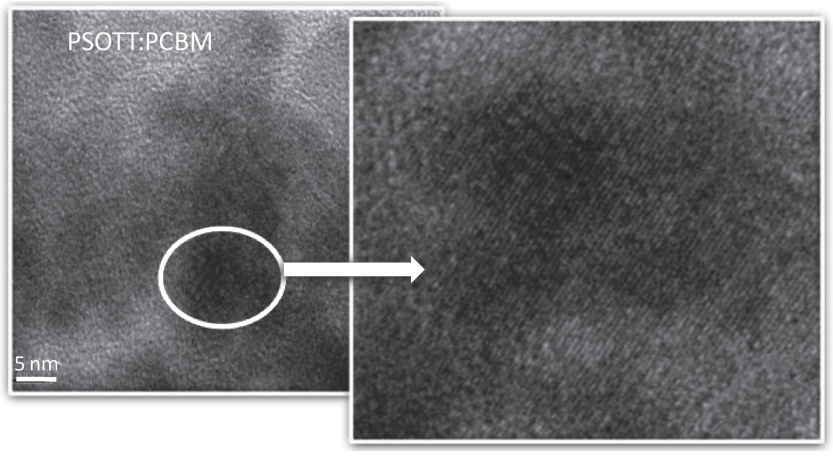

Figure 2. High-resolution TEM (HRTEM) image of PSOTT:$PC_{71}BM$ blend, stained with RuO_4. Dark regions correspond to the polymer. The expansion on the right clearly shows lattice fringes with ≈2 nm spacing, consistent with the lattice spacing of PSOTT determined from XRD data.[17]

We turn now to consideration of fullerene aggregation/crystallinity. XRD data for neat $PC_{71}BM$ and ICBA films is shown in the inset to Figure 1a. It is apparent that ICBA lacks the peaks at 17–20° and 25–30° previously assigned to the formation of aggregated PCBM domains.[40] Further evidence for the lower tendency of ICBA to crystallize/aggregate comes from optical absorption data, as shown in **Figure 3**, which shows spectra for neat films of both fullerenes and their blends with polystyrene. Previous studies have shown that $PC_{61}BM$ is highly miscible with polystyrene, with the addition of polystyrene preventing the formation of $PC_{61}BM$ aggregates or crystallites.[41] This change in aggregation state is clearly visible in optical absorbance data, with neat $PC_{61}BM$ film showing substantially greater visible light absorption than dilute blend films.[41] Analogous behavior was observed for $PC_{71}BM$, as shown in Figure 3a, with the neat film showing a clear red shift of its optical absorbance relative to the blend film with polystyrene, indicative of strong electronic interactions between $PC_{71}BM$ molecules. In contrast, the absorption spectra of neat and blend films of ICBA are relatively invariant (and similar to solution spectra), indicative of its low tendency to aggregate/crystallize. A similar conclusion can be drawn from film cyclic voltammetry data. We have previously shown that the dilution of $PC_{61}BM$ in polystyrene results in a 100–200 meV shift in its electrochemical reduction wave, indicative of a decrease of its electron affinity with decreased aggregation.[10] A similar shift of $PC_{71}BM$ reduction was observed following blending with polystyrene (**Figure 4**) and with PCPEHTT (see Supporting Information), corresponding to an 100–200 mV decrease in $PC_{71}BM$'s

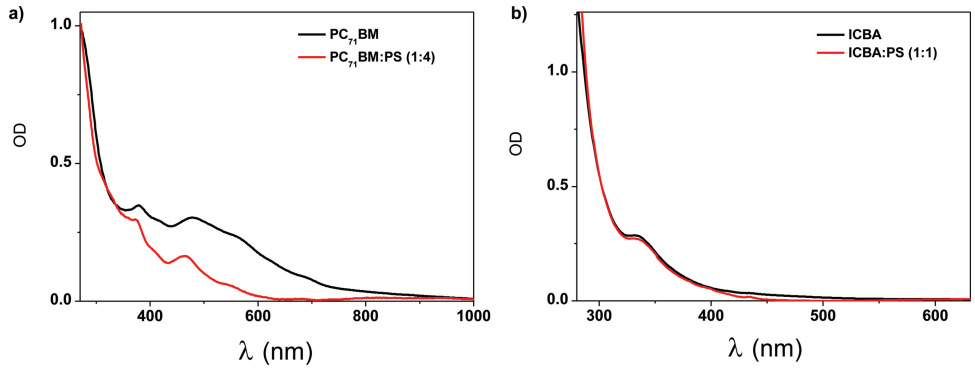

Figure 3. Ground state absorption of neat fullerene and fullerene:polystyrene blend films.

electron affinity in the blend film relative to neat $PC_{71}BM$. An analogous shift in $PC_{61}BM$ electron affinity with aggregation has also been reported from studies of charge transfer state emission of PPV/$PC_{61}BM$ blend films.[42] In contrast, comparison of cyclic voltammetry data for neat ICBA films and blends with either polystyrene or PCPEHTT (Figures 4 and Supporting Information, respectively) indicate that ICBA's electron affinity is unchanged by blending, consistent with its lower tendency to form relatively aggregated or crystalline domains even in neat films. This difference in the dependence of fullerene upon electron affinity upon blending is also consistent with electroluminescence studies of analogous polymer:$PC_{61}BM$ and polymer:ICBA films.[13] The lower tendency of ICBA to aggregate relative to $PC_{71}BM$ is consistent with previous reports that fullerene bis-adducts such as ICBA tend to show lower crystallinity than monoadducts such as $PC_{61}BM$, assigned at least in part to the presence of several isomers in such bis- and higher adducts which increases structural disorder.[43] The relevance to photovoltaic function of this difference in aggregation/energy level behavior between the two fullerenes is discussed further below.

2.2. Photophysical Analyses of Charge Photogeneration

All of the polymers studied exhibited rather similar absorption spectra and optical bandgaps (see Supporting Information) such that the differences in J_{SC} cannot be assigned primarily to differences in light absorption by the blend films. $PC_{71}BM$ does exhibit higher blue light absorption than ICBA, which can be expected to result in a modest enhancement in light absorption for $PC_{71}BM$ blend films (of the order of 1–2 mA cm^{-2}). However, in this paper, we focus rather on the efficiency of charge generation from photogenerated excitons in these blend films.

We consider first the efficiency of polymer exciton quenching in the blend films. The extent of polymer emission quenching of the polymer/fullerene blend film relative to the corresponding neat polymer film can be a useful assay of polymer exciton quenching, assigned to electron transfer from the polymer exciton to the fullerene acceptor. Typical emission quenching data are shown in the supporting information, and summarized for all the blend films studied in Table 1. It is apparent that polymer emission is strongly quenched (>90%) for all the blend films studied, consistent with reasonably large energy offsets driving charge separation for all the blend films studied. As such we conclude that exciton quenching is not a significant factor limiting charge generation for any of the blend films studied herein. It is furthermore apparent from Table 1 that the polymer emission quenching is slightly reduced for blend films of the crystalline polymers (≈90%) compared to that observed for the amorphous polymer PCPEHTT (≈99%), independent of acceptor fullerene. As we have discussed previously for other donor polymers,[10] this difference can be assigned to the

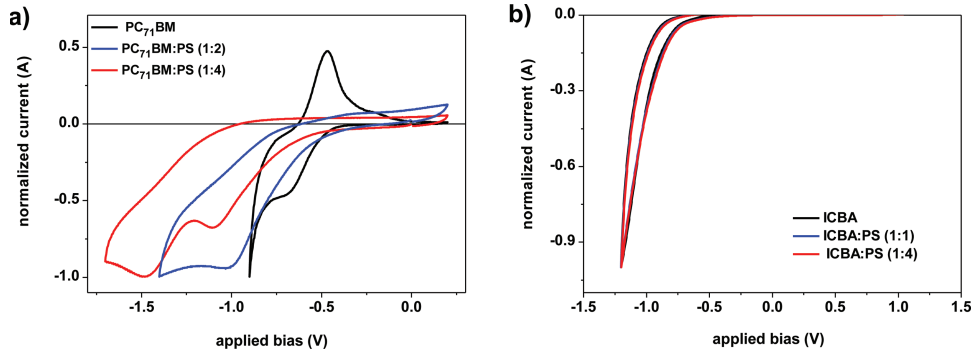

Figure 4. Film cyclic voltammetry data for a) neat $PC_{71}BM$, 1:2 and 1:4 polystyrene blend films. b) neat ICBA and 1:1 and 1:4 polystyrene blend film. Data collected using ferrocene/ferrocenium (Fc/Fc+) and plotted versus SCE.

formation of relatively large crystalline, pure polymer domains on the same length-scale as the exciton diffusion length (≈10 nm) for the crystalline polymers, consistent with the XRD and TEM data above. In contrast, the very high emission quenching for the amorphous polymers such a PCPEHTT is indicative of intimate mixing of the polymer and fullerene,[10,44] again consistent with the TEM data, without the formation of significant polymer only domains.

We turn now to consideration of the yield of dissociated charges in the blend films studied herein. We have previously demonstrated that nano-millisecond transient absorption spectroscopy can be an effective assay of the yield of dissociated charge carriers[23,45] and their recombination dynamics[46] in organic donor/acceptor blend films. The technique monitors the transient absorption of photogenerated charge carriers following low intensity, pulsed laser excitation. Geminate recombination can be readily distinguished from non-geminate recombination by consideration of the timescale, excitation density dependence and functional form of the decay dynamics (exponential for geminate recombination and power-law for non-geminate recombination). This technique can thus be employed to assay the overall efficiency of charge photogeneration in such blend films. This contrast with the emission quenching assay, which monitors only the efficiency of exciton dissociation, but is however unable to assay whether the initially generated charges at the donor/acceptor interface dissociate into free charges or undergo geminate recombination.

Typical transient absorption data for PCPEHTT:ICBA and PCPEHTT:$PC_{71}BM$ blend films are shown in **Figure 5**. Data for PCPEHTT:$PC_{71}BM$ are typical of those observed for all the other blend films studied (see Supporting Information and also ref. [17]); data for PCPEHTT:ICBA is anomalous, as we discuss below. Data were collected at a probe wavelength of 730 nm, assigned as previously to the absorption maxima of polymer polarons for all the donor polymer studied herein (see Supporting Information for typical spectra of these polaron absorption).[47,48] In all blend films, the transients exhibited oxygen-independent decay dynamics, consistent with their assignment to polaron rather than triplet absorption. Control data on all neat polymers films gave negligible transient signals on the timescales studied. For all blend films studied, sufficiently low excitation densities were employed such that the initial signal amplitude were observed to vary approximately linearly with excitation density (see Figure 5b,c and Supporting Information), indicating that saturation effects do not distort signal comparisons. All transient signals were normalized for variations in the density of absorbed photons due to variations in film optical density at the excitation wavelength, thus allowing comparison of signal amplitudes between blend films.

With the exception of PCPEHTT:ICBA, all blend films gave long-lived power-law ($\Delta OD \propto t^{-\alpha}$) decay dynamics corresponding to a straight line on the log/log plot, as illustrated in Figure 5b and typical of those we have reported previously for other polymer/fullerene blend films.[46] As we have discussed extensively previously,[22,49] and confirmed by numerical modelling,[50] such power law kinetics on the nano- to millisecond timescales are characteristic of non-geminate recombination of dissociated charge carriers. At low excitation densities, a plateau is observed at early times, consistent with observation of the onset of non-geminate recombination. At high excitation densities, the power law decay phase saturates in amplitude and an additional fast decay phase is observed, assigned, as previously,

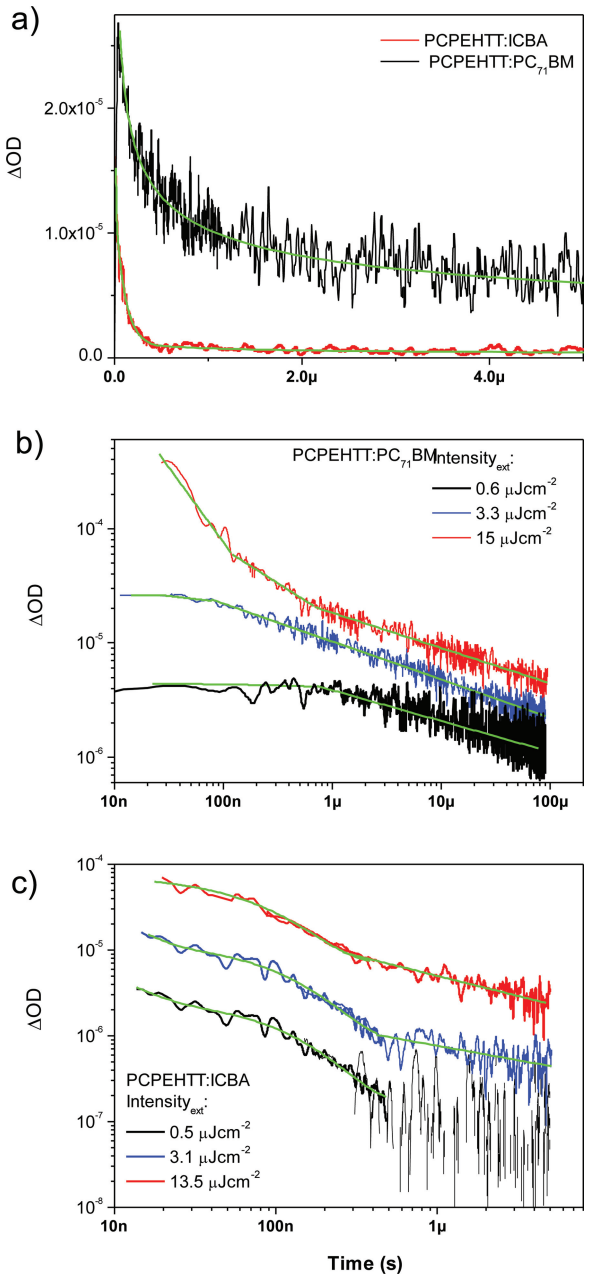

Figure 5. a) Comparison of transient absorption data for 1:1 blend films of PCPEHTT with ICBA and PCBM, plotted on linear axes (at 3 μJ cm^{-2}). b) The corresponding data for the PCPEHTT:PCBM blend films as a function of excitation density, showing a clear power law decay (straight line on the log:log plot used), with an additional faster decay phase, assigned to free carrier non-geminate recombination, only being observed at high excitation densities. Analogous data were obtained for all the blend films studied here where either or both of the materials exhibit some crystallinity. c) Analogous data for the amorphous PCPEHTT:ICBA blend film, exhibiting a biphasic decay at all excitation densities, comprising a monoexponential ($\tau \approx 100$ ns) decay followed by a relative small power-law decay. All data obtained following excitation at 560 nm, probed at 730 nm under N_2 atmosphere.

to non-geminate recombination of un-trapped (free) polarons.[50] This free carrier recombination is observed only at high excitation densities and will not be considered further herein. As previously, we have employed the initial amplitude of this power law decay, measured under low excitation conditions prior to the onset of non-geminate recombination losses, as a quantification of the quantum yield of dissociated charge carriers in such blend films (determined at 20 ns, extrapolating back the power law decay where necessary). Amplitudes of the initial amplitudes of these power law decays are listed in Table 1. It is apparent that there are significant variations in the amplitudes of these initial signals, indicative of variations in the yield of dissociated charge between blend films. We consider the correlation between these amplitudes and the observed photocurrent below.

The behavior of the PCPEHTT:ICBA blend films is more complex and differs from all the other blend films studied herein by exhibiting a clear bi-phasic behavior even at low excitation conditions, as shown in Figure 5c. For most of the polymers studied herein, the transient absorption data collected with ICBA and PCBM were very similar (see Supporting Information and ref. [17]). However for PCPEHTT, the blend with ICBA exhibits in addition to the power-law phase apparent at long times, an additional fast, monoexponential decay phase (lifetime of 110 ± 10 ns). The amplitude of this fast decay phase scaled linearly with excitation density, with no change in lifetime, as illustrated in Figure 5c. This behavior suggests that this 100 ns decay phase should be assigned to geminate rather than non-geminate recombination of photogenerated charge carriers. We have also observed similar behavior for another (also relatively amorphous) donor polymer, PCDTBT blended with ICBA. (see Supporting Information and ref. [46]). We note that it is not possible to completely rule out some contribution of polymer triplet exciton absorption to this 100 ns exponential decay phase. However, comparison with neat film data, which exhibited no triplet signals, suggesting that any triplets generated in this polymer decay on timescales faster than our time resolution, suggests that this is unlikely. In addition our energetic correlations, presented below, provide further support for assignment of this decay phase to geminate recombination of photogenerated polarons. We consider further below the impact of this recombination phase upon device performance.

3. Discussion

We have reported above a study of photophysics, microstructure and energetics of fullerene films blended with a particular series of polymers, which only differ in their side groups and bridging atoms, affecting the crystallinity of the neat and blend films. These results are compared against device short circuit photocurrent densities in Table 1. We next discuss the quantitative correlations between these data, and implications for materials function.

3.1. Correlating Photocurrent Densities with the Yield of Photogenerated Polarons

We consider first whether, for the materials studied herein, there is a correlation between our transient absorption assay

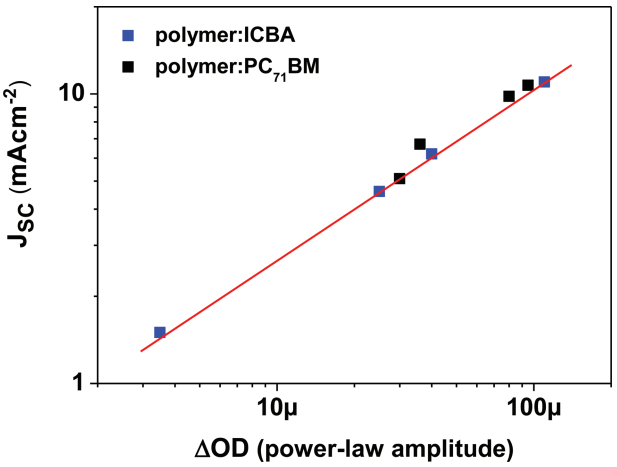

Figure 6. Plot of the amplitude of the power law decay phase observed in transient absorption studies and assigned to dissociated polarons versus the J_{SC} measured in complete devices under simulated AM 1.5 irradiation. Data are shown for both polymer:$PC_{71}BM$ (■) and polymer:ICBA (■) blends. The amplitude of the power law decays was determined at 20 ns, extrapolated back where necessary. All data were taken at a laser intensity of 3 μJ cm^{-2}.

of charge photogeneration (measured on the nano- to microsecond timescales) and device photocurrent. We have previously reported a clear correlation between device photocurrent and the amplitude of the power law transient absorption decay phase, assigned to the photoinduced absorption of dissociated charge carriers in the blend films, for a range of donor polymers blended with $PC_{60}BM$ and $PC_{70}BM$.[45] The result of this analysis for the fullerene:polymer set studied herein is shown in **Figure 6**. It is striking that for the blends studied herein we observe a good correlation between the amplitude of our power-law decay phase and J_{SC}. This correlation suggests that the photocurrent density in this series of OPV devices is largely determined by the yield of dissociated charges measured in the corresponding blend films. This observation indicates that, for all the blend films studied herein, collection of dissociated charge carriers by the device electrodes is relatively efficient under short circuit conditions (i.e., that for all the devices studied, non-geminate recombination losses are not the primary determinant of J_{SC}). It also suggests that yields of dissociated charges are similar in blend films and devices, indicating that the electric fields present in the devices due to electrode charge are not the primary determinant of charge dissociation.

The correlation we observe between J_{SC} and the amplitude of the power-law decay phase includes the blend film of the donor PCPEHTT polymer with ICBA. As we discuss above, the biphasic recombination observed for this blend film is assigned to the presence, in addition to the power law decay phase of dissociated charges, of an additional, relatively fast (≈100 ns) exponential decay phase assigned to a geminate recombination process. The photocurrent generation observed for this blend film is in reasonable agreement with the amplitude of the power-law decay phase for the film (extrapolated back to 20 ns as for the other films). However it does not correlate with the initial signal amplitude including both the exponential and power law decay phases. This observation indicates that for this

blend film, charge carriers which decay by the 100 ns exponential decay phase do not result in efficient photocurrent generation. Supporting this conclusion, we note that PCDTBT:ICBA blend films, which also exhibit this 100 ns decay phase,[13] also yield poor device photocurrents. This conclusion is consistent with assignment of this 100 ns decay phase to the geminate recombination of weakly associated charge pairs, who therefore are unable contribute significantly to photocurrent generation.

3.2. Correlating the Initial Polaron Yield with the Energy Offset Driving Charge Separation

In the preceding paragraphs we have shown that device photocurrent density correlates with the amplitude of the yield of dissociated charge carriers measured in blend films. We turn now to consideration of what materials properties determine this yield of dissociated charges. We have previously shown that for several materials series, this yield correlates with the energetic driving force for charge separation, $\Delta E_{CS}^{eff} = E_S - (IP - EA)$, where E_S is the energy of the polymer singlet exciton, IP the ionization potential of the donor and EA the electron affinity of the acceptor.[22–23,51] Values for ΔE_{CS}^{eff} are detailed in Table 1 and discussed further below. In **Figure 7** we plot our transient absorption assay of the initial polaron yield, measured from transient absorption signal amplitude measured at 20 ns, ΔOD_{20ns}, versus this energy offset ΔE_{CS}^{eff}. In plotting these data, there are two key considerations, which are apparent for the results reported herein but which have previously not been addressed in detail. The first concerns the biphasic decay kinetics observed for the PCPEHTT:ICBA blend–and whether the energy offset correlates specifically with the initial polaron yield ΔOD_{20ns}, or the yield of the power law decay phase alone; this point will be discussed further below. Secondly, we note that our determination of ΔE_{CS}^{eff} includes consideration of the impact of materials blending upon reduction/oxidation potentials as indicated by our film cyclic voltammetry data, as we discuss below. It is apparent from Figure 7 that we observe a strong correlation between our ΔOD_{20ns} assay of the initial polaron yield and the energy offset driving this charge separation ΔE_{CS}^{eff}. This correlation is consistent with our previous observations, and with charge separation models where a larger ΔE_{CS}^{eff} increases the excess energy of the initially injected electron, thereby enabling it overcome its coulomb attraction with the positive polymer polaron,[22–23] most probably associated with an increase in wavefunction delocalization.[26]

As indicated above, the values of ΔE_{CS}^{eff} employed in Figure 7 take account of the shifts in polymer IP and acceptor EA observed from our cyclic voltammetry studies, as detailed in Supporting Information. In particular, we have included a 175 meV increase in IP for PCPEHTT relative to its literature value as indicated by the shift in oxidation waves between neat polymer and blends films. No increase was applied to the IPs of the other donor polymers as indicated by the CVs for neat and blend films with PSOTT. For the two fullerenes, our film CV data for the neat films indicate that $PC_{71}BM$ exhibits a 140 ± 25 mV higher EA than ICBA, consistent with literature data. However, for the blend films, the shift in $PC_{71}BM$ reduction wave observed relative to the neat film results in the reduction wave for $PC_{71}BM$ being only 20 ± 25 mV less negative than ICBA (see Supporting Information for a comparison of the ICBA and $PC_{71}BM$ reduction data shown in Figure 4 and discussion of this rather surprising observation[52]). A correlation between ΔOD_{20ns} and ΔE_{CS}^{eff} was also apparent if we employed values for IP and EA taken directly from literature values, without consideration of the energy shifts associated with the changes in energetics indicated by our cyclic voltammetry data (see Supporting Information), although in this case the correlations are limited to subsets of the full data set. As such, the results reported herein emphasise the importance of in situ measurements of materials energetics directly in blend films over ex situ measurements in neat films or dilute solution when undertake detailed analysis of materials OPV function, as has been discussed elsewhere using range of different in situ techniques.[20,21,53–55]

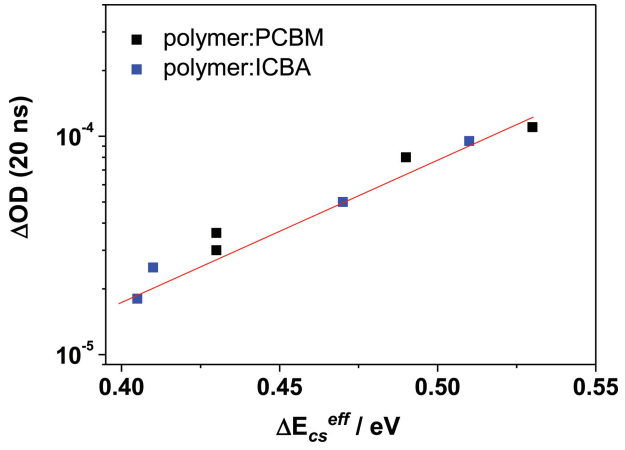

Figure 7. Plot of the initial amplitude (measured at 20 ns, 3 μJ cm^{-2}) of the transient absorption signal assigned to the polaron absorption versus the energy offset driving charge separation determined from materials energy levels measured from blend films data.

3.3. Origin of the 100 ns Geminate Recombination Decay

We next consider the origin of the 100 ns decay phase observed for the PCPEHTT:ICBA blend films. This decay phase scales linearly with excitation density, and exhibits monoexponential behavior, indicating it should be assigned to geminate rather than non-geminate recombination. The analysis of charge photogeneration versus energy offset for the materials studied herein, as plotted in Figure 7, uses the initial amplitude of the photogenerated charges, as assayed by the transient absorption signal measured at 20 ns, and including both the amplitudes of both the exponential and power-law decay phases. If only the power-law decay phase amplitude is used, then the data for the PCPEHTT:ICBA blend film deviates very clearly from that of ΔOD versus ΔE_{CS}^{eff} observed for the other films (see Supporting Information). This contrasts with the correlation between ΔOD and J_{SC} shown in Figure 6, where a clear correlation (including this film) was only observed by using the power law decay amplitude and not the total initial amplitude. This difference

in behavior provides further support for our assignment of the 100 ns exponential decay phase to a geminate recombination process. It appears that the energy offset ΔE_{CS}^{eff} is the primary determinant of the initial charge generation observed in our experiments; in other words the primary determinant of the efficiency of the initial charge generation, and any geminate recombination losses occurring on timescales faster than our time resolution (<20 ns). These sub-nanosecond geminate recombination losses can most probably be assigned to the formation and decay of bound interfacial charge transfer states. For most of the films studied, all of the polarons observed on the 20 ns and longer timescales are dissociated, and capable of generating photocurrent. However for PCPEHTT:ICBA film, most of the charges observed at 20 ns are not fully dissociated, but rather undergo geminate recombination on the 100 ns timescale, preventing efficient photocurrent generation.

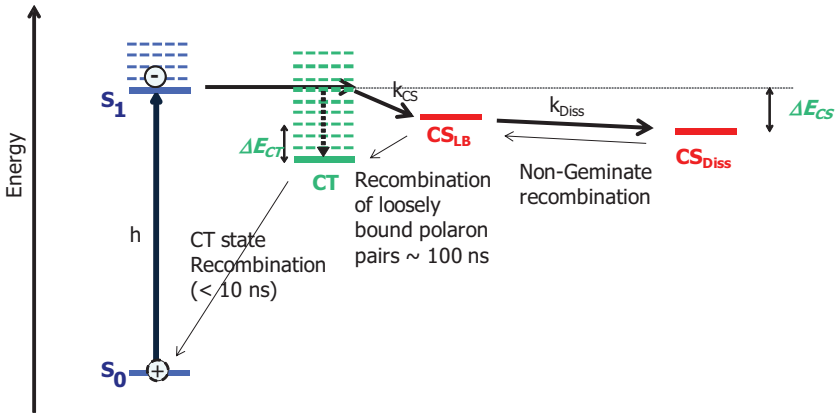

Figure 8. Illustration of model of charge separation from polymer singlet excitons, including both interfacial CT states, loosely bound polaron pairs CS_{LB} and dissociated polarons CS_{Diss}. The yield of polarons is determined by the branching between k_{CS} and relaxation to bound CT states (the vertical black dashed line), which subsequently undergoes rapid geminate recombination. For blend films where at least one material is relatively crystalline, efficient dissociation of photogenerated polarons is observed (k_{Diss}). For amorphous blend films, significant recombination of loosely bound polaron pairs is observed on the 100 ns timescale. This diagram does not include the additional stabilization of the dissociated polaron energy associated with their increased entropy, which corresponds to relaxation of their free energy down to the blend quasi-Fermi levels.

At present we are unclear whether the geminate recombination we observe herein on the ≈100 ns timescale corresponds to the recombination of weakly coulombically bound radical pairs, or the recombination of polaron pairs which have escaped their coulomb attraction but remain physically confined by the physical size of their respective domains. We note that picosecond timescale geminate recombination has been previously reported in range of polymer/fullerene blend films.[14,56] On the other hand, geminate recombination dynamics of coulombically bound, emissive charge transfer states in polymer/polymer blends (sometimes referred to as exciplexes) have been reported to occur on the ≈50 ns timescale.[57] Pal et al.[58] have also reported geminate charge recombination occurring on the nanosecond time scale for a range of polymer:fullerene BHJ films. We have observed a similar 100 ns monoexponential decay in small-molecule: $PC_{61}BM$ blend films where this recombination loss was strongly bias dependent,[59] and in a polymer/fullerene blend where the fullerene was highly miscible with the polymer, resulting in negligible phase segregation.[46] Notwithstanding these uncertainties over the physical origin of the 100 ns geminate recombination decay phase observed herein, we will refer hereafter to this recombination as geminate recombination of loosely bound polaron pairs.

3.4. A Kinetic Model of Charge Separation

A kinetic model of charge separation consistent with the data reported herein is illustrated in **Figure 8**. This figure model includes the presence of interfacial CT states and loosely bound polaron pairs. As we have discussed previously,[22,23] the dependence of the observed polaron yield upon ΔE_{CS}^{eff}, as observed herein in Figure 7, is indicative of a charge separation model whereby excess (thermal or electronic) energy of electrons injected into the fullerenes is required to enable them to overcome their coulomb attraction to the polymer polaron, and thereby avoiding forming a bound, relaxed interfacial CT state. Figure 8 extends this model for the material set studied herein by including loosely bound polaron pairs, as an additional intermediate in the charge separation process. Such loosely bound polaron pairs are observed for the results reported herein for the amorphous film, where they are observed to recombine with a 100 ns lifetime. For the blends films where one or both materials exhibit significant crystallinity, this decay phase is not observed, suggesting that such loosely bound polaron pairs either are not formed or, more likely, readily separate into dissociated polarons. This final dissociation process is stabilized both by the increased entropy (higher degeneracy) of dissociated polarons and by relaxation of these polarons into lower energy regions of the film (e.g., localized traps etc).

We note the model illustrated in Figure 8, as well as being consistent with the data reported herein, may allow us to reconcile some apparently conflicting data in the literature concerning the excess energy requirement for charge separation. In particular, Zhou et al.[60] have considered a similar model for donor–acceptor pairs in solution, and shown that charge separation following sub-bandgap excitation in such systems can derive primarily from direct excitation of loosely bound radical ion pairs, analogous to loosely bound polaron pair states shown in Figure 8. As such, it is possible that recent reports[15,61–62] of efficient charge dissociation following sub-bandgap excitation in polymer/fullerene blends may derive primarily from direct optical excitation of these loosely bound polaron pair states.

3.5. A Structural and Energetic Model of Charge Photogeneration

We next consider why the PCPEHTT:ICBA blend film alone exhibits this 100 ns geminate recombination decay phase, and as a consequence particularly poor photocurrent generation.

We note the appearance of this 100 ns geminate recombination only for PCPEHTT:ICBA blend cannot be assigned to interfacial energetics, as PCPEHTT's ΔE_{CS}^{eff} is similar to that PSOxTT. PCPEHTT's ΔE_{CS}^{eff} is similar to that PSOxTT after taking account of the increase in PCPEHTT's IP in blend films relative to neat films. If neat film IP's are used, ΔE_{CS}^{eff} for PCPEHTT is actually 150 mV larger than PSOxTT. It is however interesting that PCPEHTT is significantly more amorphous than the other donor polymers studied. In this regard, we have observed an analogous 100 ns decay phase for blend films of the amorphous polymer PCDTBT with ICBA, but not for films of the crystalline polymer P3HT with ICBA.[63] In addition, several groups have noted a correlation between the ability of blend films with ICBA to generate photocurrent and donor polymer crystallinity.[12,64–66] It thus appears plausible to relate the appearance of this decay phase to the relatively amorphous nature of both the donor and acceptor materials in this blend.

We have previously argued that the tendency of $PC_{61}BM$ to form crystalline or aggregated domains with a higher electron affinity may be a key factor in stabilizing the spatial separation of charges in polymer:$PC_{61}BM$ blend films,[10] and thereby a key factor behind the success of PCBM as an acceptor in BHJ solar cells. We consider further this factor with regard to the materials series studied herein. This concept is illustrated in **Figure 9**, which illustrates three different structure/function models depending upon materials crystallinity/miscibility. In Figure 9a, corresponding to blend films with a crystalline polymer, crystallization of the donor polymer results in the formation of relative pure, distinct polymer and fullerene phases. The model also indicates some reduction in material crystallinity at the polymer/fullerene interface, which may function to generate energy gradients to aid movement of polarons away from this interface, as has been discussed elsewhere.[67] In this model, excitons diffuse to and are dissociated at the interface between polymer and fullerene domains, resulting in a clear spatial separation of electrons and holes, and reasonably slow non-geminate recombination enabling efficient charge collection. This model corresponds to the conventional model typically used to describe bulk heterojunction device function. In Figure 9c, corresponding to blends of an amorphous polymer with $PC_{71}BM$, the blend film comprises primarily an amorphous mixed polymer/fullerene phase alongside aggregated $PC_{71}BM$ domains. Photogenerated polymer excitons formed in the mixed phase separate into polarons by electron transfer to $PC_{71}BM$ molecules within this phase (either as fully separated states or loosely bound polaron pairs). These polarons are spatial separated when the $PC_{71}BM$ electron moves into an aggregated $PC_{71}BM$ domain, where the higher $PC_{71}BM$ electron affinity in the aggregated domain stabilizes the electron on this phase, spatially separating the electrons and holes, and thus again enabling charge separation with a lifetime sufficient for charge collection. The model shown in Figure 9b) corresponding to blends of an amorphous polymer with ICBA, is analogous to the model in Figure 9c except that there is no difference in fullerene electron affinity between the mixed and fullerene rich domains, thus there is no energetic offset to spatially separate the charges. As such, whilst photogenerated electrons may diffuse to ICBA rich domains (if present), there is no interfacial energy offset which stabilizes the electrons on these domains. As a consequence, photogenerated electrons and holes would not be spatially separated into distinct domains, resulting in rapid electron/hole recombination on the 100 ns timescale, as observed.

The structure–function model shown in Figure 9 provides a simple explanation for why the ICBA acceptor fullerene only exhibits efficient photovoltaic performance with relatively crystalline polymers,[12,64–65] while $PC_{71}BM$ can exhibit efficient device performance with both crystalline and amorphous donor polymers. ICBA exhibits a similar reduction potential in neat and blend films, indicating that any ICBA aggregation

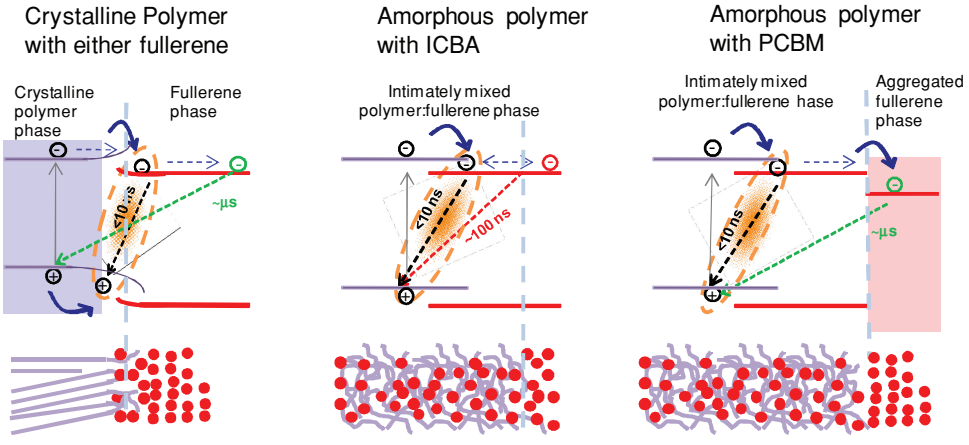

Figure 9. Illustration of the functional model proposed herein, where the blend film is considered to comprise a relatively amorphous, intimately mixed polymer/fullerene phase as well as, for materials which exhibit sufficient crystallinity, relatively crystalline, chemical pure phases. These crystalline domains exhibit a smaller IP (for donor materials) and larger EA (for acceptor materials). The interface between the mixed and crystalline domains thereby provides an energy offset which can stabilize the spatial separation of charge carriers. The model is illustrated for blend films comprising a relatively crystalline donor polymer (a), relatively crystalline acceptor fullerene (c), or where neither polymer nor fullerene exhibit significant crystallinity (b). In (b) the absence of a well defined interface to separate polarons results in relatively rapid charge carrier recombination, preventing efficient photocurrent generation.

present in blend films does not result in a shift in its electron affinity. As such, spatial separation of photogenerated charges in polymer/ICBA blend films is dependent upon the formation of relatively pure, crystalline polymer domains with relatively low ionization potentials, such that positive polarons are localized in this crystalline polymer domain. For amorphous donor polymers, the lack of these crystalline polymer domains results in rapid electron/hole recombination (the 100 ns decay phase observed herein) and low photocurrent generation. The ability of $PC_{71}BM$, but not ICBA, to function as an effective electron acceptor in blends with amorphous donor polymers can then be understood as resulting from the greater tendency of PCBM to form crystalline or aggregated domains with higher electron affinities. These crystalline $PC_{71}BM$ domains stabilize the spatial separation of charges in blend films, with this stabilization being particular critical for efficient photocurrent generation in blend films with amorphous donor polymers. We note this model is also consistent with the typical observation that OPV devices of amorphous polymers with PCBM typically requires relatively high weight percentages of fullerene, with this excess fullerene being necessary to ensure the solubility limit for PCBM in the polymer is exceeded, resulting in the formation of aggregated PCBM domains. We further note this model implies that for some BHJ devices, and particularly those employing amorphous donor polymers, the spatial separation of photogenerated charge carriers into separate domains is driven not by an energy offset between the HOMO and LUMO levels of different donor and acceptor materials but rather by a LUMO level offset generated by a change in aggregation state of the single acceptor material. This alternative mechanism for spatial separating charges in BHJ devices clearly has implications for the design of materials, and particularly acceptor materials, in such OPV devices.

4. Conclusions

The study reported in this paper, albeit limited in the range of materials studied, does provide new insights into materials design guidelines for bulk heterojunction solar cells. The conclusions we draw from our observations, which build upon our previous studies,[10] emphasis that functional models of BHJ devices must include consideration of not only phase separated polymer and fullerene domains, but also molecularly mixed amorphous domains. They suggest that for blend films with significant molecular mixed, amorphous domains, kinetic models of charge separation based upon CT and charge separated states are inadequate to explain fully device function, but must also include consideration of intermediate loosely bound polaron pairs.

Our results suggest that, for the materials series studied, materials crystallinity can influence device photocurrent generation in two ways: 1) structural control through the formation of relatively pure, crystalline donor or acceptor domains alongside more amorphous, finely mixed donor/acceptor domains and 2) energetic control with the more crystalline domains exhibiting lower ionization potentials and higher electron affinities than the more amorphous domains. By employing material energetics which takes some account of the differences in crystallinity associated with blend formation, we observe a clear correlation between the yield of charges observed at 20 ns and the energetic driving force driving charge separation, ΔE_{CS}, independent of blend crystallinity. As such, the yield of charge separation at 20 ns appears to be primarily dependent upon materials energetics, including the impact of material crystallinity upon its energetics, but is otherwise rather independent of materials crystallinity per se, at least for the materials studied herein. In contrast, our data suggest the ability of these charge carriers to generate photocurrent does appear to be dependent upon materials crystallinity. In amorphous blend films, which lack the presence of significant fractions of crystalline domains to act as energetic sinks to stabilize spatial charge separation, we suggest that charge carriers may be susceptible to recombination on a timescale (≈100 ns) too fast to allow effective collection by the external circuit.

These results have important implications for the role of materials structure in the function of BHJ solar cells. They emphasis the role of amorphous, relatively mixed domains in achieving exciton quenching and charge generation, and the role of crystalline domains in stabilising charge separation and enabling efficiency charge carrier collection.

5. Experimental Section

Thiazolo-thiazole polymers were synthesized as reported previously.[17,18] The number average molecular weight (M_n) of PCPEHTT is 8.0 kDa and polydispersity index (PDI) is 1.46. All polymers were blended with either $PC_{71}BM$ or ICBA. $PC_{71}BM$ was purchased from Solenne and ICBA was supplied by Plextronics. All materials were used as received.

ITO-coated glass substrates (24 Ω per square from Psiotec) were cleaned in acetone and isopropyl several times and then finally blow dried with nitrogen. Cleaned ITO substrates were transferred for oxygen plasma treatment and were treated for 7 min under an oxygen pressure of 0.25 mbar. On the top of the treated ITO, poly(styrenesulfonate) (PEDOT:PSS) (Baytron P, VP AI 4083 grade, HC Stark) was spin-coated at 3500 rpm, before being soft-baked at 150 °C for 20 min.

For the thiazolo-thiazole:fullerene active layer, polymer and fullerene ($PC_{71}BM$ or ICBA) solutions were prepared separately with concentrations of 6 mg/mL and 12 mg/mL respectively in ODCB. Polymer solution was left on the hot plate at 100 °C under constant stirring in the glove box and filtered through 0.45 μm filter before mixing with equal volume of fullerene solution. The blend solution was left in the glove box for an hour at 100 °C before spinning on substrate. The active layer of polymer:fullerene blend films were spin coated (on glass or PEDOT:PSS layer) at spin speed of 680 rpm in the glove box. The active layer films were kept in the vacuum chamber for an hour and finally LiF (≈10 nm) and Aluminum (1000 nm) electrodes were evaporated under vacuum 2.0×10^{-6} mbar, defining an active device area of 0.045 cm^2.

Device efficiencies and *J–V* characteristics were measured by using Keithley 238 Source Measure Units. Illumination was provided using a 300 W xenon arc lamp solar simulator (Oriel Instruments) and calibrated using a silicon photodiode in order to ensure the illumination intensity of 100 mW/cm^2, at 1 sun AM 1.5. The J_{sc} measurements were cross checked with the calculated J_{sc} obtained from the integrated EQE spectrum. During the measurements, the devices were kept in nitrogen environment in a sealed chamber. Transient absorption decays were measured by exciting the sample film, under a nitrogen (and oxygen) atmosphere, pumped with a Nd:YAG laser (Lambda Photometrics). The excitation wavelength used was 560 nm, with a pump intensity of 0.4–50 μJ cm^{-2} and a repetition frequency of 20 Hz. For 1 μs–100 μs timescale, a 100 W quartz halogen lamp (Bentham, IL 1) with a stabilized power supply (Bentham, 605) was used as the probe light source. For the faster timescale data, a photodiode

(Thorlabs ITC502) was used as the probe. The probe light passing through the sample film was detected with a silicon photodiode (Hamamatsu Photonics, S1722-01). The signal from the photodiode was pre-amplified and sent to the main amplification system with an electronic band-pass filter (Costronics Electronics). The amplified signal was collected with a digital oscilloscope (Tektronics, TDS220), which was synchronized with a trigger signal of the pump laser pulse from a photodiode (Thorlabs Inc., DET210). To reduce stray light, scattered light and sample emission, two monochromators and appropriate optical cut-off filters were placed before and after the sample. For TEM examination, solutions were prepared on PEDOT:PSS coated substrates and then retrieved on carbon-coated copper grids. The sample film thickness was controlled by the solution concentration, typically around 30 nm. The samples were then stained by RuO_4 vapour. Wide-angle X-ray scattering (WAXS) were carried out with a PANALYTICAL X' PERT-PRO MRD diffractometer equipped with a nickel-filtered Cu-$K_{\alpha 1}$ beam and X' CELERATOR detector, using current I = 40 mA and accelerating voltage U = 40 kv. Measurements were performed on drop cast solutions of 10 mg/mL concentration on glass substrates. Electrochemical measurements were carried out between +1.5 V and –1.9 V for each film, employing a 0.1 M tetrabutylammonium perchlorate (Alfa Aesar) in acetonitrile (Aldrich) electrolyte. Data are shown for a scan rate of 70 mV s^{-1}. The counter and reference electrodes were Pt and Ag/AgCl respectively. Ferrocene/ferrocenium (Fc/Fc^+) and standard calomel electrode (SCE) were separately used as internal standards, with all data being plotted relative to SCE.

Supporting Information

Supporting Information is available from the Wiley Online Library or from the author.

Acknowledgements

The authors are grateful to the EPSRC Apex, EP/H040218/1 and Supergen EP/G031088/1 programmes and Solvay S.A. for funding, Plextronics and Professor YongFang Li for supply of ICBA, and Jenny Nelson, Mark Faist, and Thomas Kirchartz for helpful discussions on CT states, Akshay Rao and Peter Hore on CT state intersystem crossing dynamics, Garry Rumbles for pointing out ref. [60]. Work at the University of Washington wass also based on work (Excitonic Solar Cells) supported by the US Department of Energy, Office of Basic Energy Sciences, Division of Materials Sciences under Award No. DE-FG02-07ER46467.

Received: October 26, 2012
Revised: December 4, 2012
Published online: February 6, 2013

[1] G. Yu, J. Gao, J. C. Hummelen, F. Wudl, A. J. Heeger, *Science* **1995**, *270*, 1789.
[2] J. Rivnay, R. Noriega, R. J. Kline, A. Salleo, M. F. Toney, *Phys. Rev. B* **2011**, *84*, 045203.
[3] W. C. Tsoi, D. T. James, J. S. Kim, P. G. Nicholson, C. E. Murphy, D. D. C. Bradley, J. Nelson, J.-S. Kim, *J. Am. Chem. Soc.* **2011**, *133*, 9834.
[4] S. T. Turner, P. Pingel, R. Steyrleuthner, E. J. W. Crossland, S. Ludwigs, D. Neher, *Adv. Funct. Mater.* **2011**, *21*, 4640.
[5] M. Pfannmoeller, H. Fluegge, G. Benner, I. Wacker, C. Sommer, M. Hanselmann, S. Schmale, H. Schmidt, F. A. Hamprecht, T. Rabe, W. Kowalsky, R. R. Schroeder, *Nano Lett.* **2011**, *11*, 3099.
[6] W. Yin, M. Dadmun, *ACS Nano* **2011**, *5*, 4756.
[7] P. E. Hopkinson, P. A. Staniec, A. J. Pearson, A. D. F. Dunbar, T. Wang, A. J. Ryan, R. A. L. Jones, D. G. Lidzey, A. M. Donald, *Macromolecules* **2010**, *44*, 2908.
[8] B. A. Collins, E. Gann, L. Guignard, X. He, C. R. McNeill, H. Ade, *J. Phys. Chem. Lett.* **2010**, *1*, 3160.
[9] W.-R. Wu, U. S. Jeng, C.-J. Su, K.-H. Wei, M.-S. Su, M.-Y. Chiu, C.-Y. Chen, W.-B. Su, C.-H. Su, A.-C. Su, *ACS Nano* **2011**, *5*, 6233.
[10] F. C. Jamieson, E. Buchaca Domingo, T. MaCarthy Ward, M. Heeney, J. Delgado, N. Martin, N. Stingelin, J. R. Durrant, *Chem. Sci.* **2012**, *3*, 485.
[11] Y. He, H.-Y. Chen, J. Hou, Y. Li, *J. Am. Chem. Soc.* **2010**, *132*, 1377.
[12] H. Xin, S. Subramaniyan, T.-W. Kwon, S. Shoaee, J. R. Durrant, S. Jenekhe, *Chem. Mater.* **2012**, *24*, 1995.
[13] M. A. Faist, S. Shoaee, T. Kirchartz, S. M. Tuladhar, G. F. A. Dibb, S. Foster, W. Gong, T. Kirchartz, D. D. C. Bradley, J. R. Durrant, J. Nelson, *Ad. Energy Mater.* in press doi: 10.1002/aenm.201200673.
[14] I. W. Hwang, D. Moses, A. J. Heeger, *J. Phys. Chem. C* **2008**, *112*, 4350.
[15] D. Veldman, O. Ipek, S. C. J. Meskers, J. Sweelssen, M. M. Koetse, S. C. Veenstra, J. M. Kroon, S. S. van Bavel, J. Loos, R. A. J. Janssen, *J. Am. Chem. Soc.* **2008**, *130*, 7721.
[16] J. W. Chen, Y. Cao, *Acc. Chem. Res.* **2009**, *42*, 1709.
[17] S. Subramaniyan, H. Xin, F. S. Kim, S. Shoaee, J. R. Durrant, S. A. Jenekhe, *Adv. Energy Mater.* **2011**, *1*, 854.
[18] S. A. Jenekhe, S. Subramaniyan, H. Xin, F. Kim, Int. Patent. PCT/EP2010/066179, 2010.
[19] M. C. Scharber, D. Mühlbacher, M. Koppe, P. Denk, C. Waldauf, A. J. Heeger, C. J. Brabec, *Adv. Mater.* **2006**, *18*, 789.
[20] K. Vandewal, K. Tvingstedt, A. Gadisa, O. Inganas, J. V. Manca, *Nat. Mater.* **2009**, *8*, 904.
[21] D. Credgington, Y. Kim, J. Labram, T. D. Anthopoulos, J. R. Durrant, *J. Phys. Chem. Lett.* **2011**, *2*, 2759.
[22] H. Ohkita, S. Cook, Y. Astuti, W. Duffy, S. Tierney, W. Zhang, M. Heeney, I. McCulloch, J. Nelson, D. D. C. Bradley, J. R. Durrant, *J. Am. Chem. Soc.* **2008**, *130*, 3030.
[23] S. Shoaee, T. M. Clarke, C. Huang, S. Barlow, S. R. Marder, M. Heeney, I. McCulloch, J. R. Durrant, *J. Am. Chem. Soc.* **2010**, *132*, 12919.
[24] W. Li, W. S. C. Roelofs, M. M. Wienk, R. A. J. Janssen, *J. Am. Chem. Soc.* **2012**, *134*, 13787.
[25] M. T. Clarke, R. J. Durrant, *Chem. Rev.* **2010**, *110*, 6736.
[26] A. A. Bakulin, A. Rao, V. G. Pavelyev, P. H. M. van Loosdrecht, M. S. Pshenichnikov, D. Niedzialek, J. Cornil, D. Beljonne, R. H. Friend, *Science* **2012**, *335*, 1340.
[27] V. D. Mihailetchi, H. X. Xie, B. de Boer, L. J. A. Koster, P. W. M. Blom, *Adv. Funct. Mater.* **2006**, *16*, 699.
[28] T. J. Savenije, J. E. Kroeze, X. Yang, J. Loos, *Thin Solid Films* **2006**, *511*, 2.
[29] M. M. Skompska, A. Szkurłat, *Electrochim. Acta* **2001**, *46*, 4007.
[30] M. Al-Ibrahim, O. Ambacher, S. Sensfuss, G. Gobsch, *Appl. Phys. Lett.* **2005**, *86*, 201120.
[31] M. M. Mandoc, W. Veurman, J. Sweelssen, M. M. Koetse, *Appl. Phys. Lett.* **2007**, *91*, 073518.
[32] B. A. Collins, Z. Li, C. R. McNeill, H. Ade, *Macromolecules* **2011**, *44*, 9747.
[33] H. Xin, X. Guo, G. Ren, M. D. Watson, S. A. Jenekhe, *Adv. Energy Mater.* **2012**, *2*, 575.
[34] X. He, B. A. Collins, B. Watts, H. Ade, C. R. McNeill, *Small* **2012**, *8*. 1920.
[35] W. C. Tsoi, S. J. Spencer, L. Yang, A. M. Ballantyne, P. G. Nicholson, A. Turnbull, A. G. Shard, C. E. Murphy, D. D. C. Bradley, J. Nelson, J.-S. Kim, *Macromolecules* **2011**, *44*, 2944.
[36] N. C. Miller, R. Gysel, C. E. Miller, E. Verploegen, Z. Beiley, M. Heeney, I. McCulloch, Z. Bao, M. F. Toney, M. D. McGehee, *J. Polym. Sci. Part B: Polym. Phys.* **2011**, *49*, 499.
[37] N. C. Miller, S. Sweetnam, E. T. Hoke, R. Gysel, C. E. Miller, J. A. Bartelt, X. Xie, M. F. Toney, M. D. McGehee, *Nano Lett.* **2012**, *12*, 1566.

[38] L. F. Drummy, R. J. Davis, D. L. Moore, M. Durstock, R. A. Vaia, J. W. P. Hsu, *Chem. Mater.* **2011**, *23*, 907.
[39] T. M. Clarke, A. M. Ballantyne, J. Nelson, D. D. C. Bradley, J. R. Durrant, *Adv. Funct. Mater.* **2008**, *18*, 4029.
[40] B. M. Ginzburg, S. Tuichiev, S. k. Tabarov, A. A. Shepelevskii, L. A. Shibaev, *Tech. Phys.* **2005**, *50*, 1458.
[41] S. Cook, H. Ohkita, Y. Kim, J. J. Benson-Smith, D. D. C. Bradley, J. R. Durrant, *Chem. Phys. Lett.* **2007**, *445*, 276.
[42] F. Piersimoni, S. Chambon, K. Vandewal, R. Mens, T. Boonen, A. Gadisa, M. Izquierdo, S. Filippone, B. Ruttens, J. D'Haen, N. Martin, L. Lutsen, D. Vanderzande, P. Adriaensens, J. V. Manca, *J. Phys. Chem.C* **2011**, *115*, 10873.
[43] J. M. Frost, M. A. Faist, J. Nelson, *Adv. Mater.* **2010**, *22*, 4881.
[44] U. Zhokhavets, T. Erb, H. Hoppe, G. Gobsch, N. S. Sariciftci, *Thin Solid Films* **2006**, *496*, 679.
[45] T. M. Clarke, A. Ballantyne, S. Shoaee, Y. W. Soon, I. McCulloch, J. Nelson, J. R. Durrant, *Adv. Mater.* **2010**, *22*, 5287.
[46] S. Shoaee, M. P. Eng, E. Espíldora, J. L. Delgado, B. Campo, N. Martín, D. Vanderzande, J. R. Durrant, *Energy Environ. Sci.* **2010**, *3*, 971.
[47] PCDTBT polaron absorption was observed to exhibit a maximum at 980 nm, consistent with literature values.[49]
[48] F. Etzold, I. A. Howard, R. Mauer, M. Meister, T.-D. Kim, K.-S. Lee, N. S. Baek, F. Laquai, *J. Am. Chem. Soc.* **2011**, *133*, 9469.
[49] J. Nelson, S. A. Choulis, J. R. Durrant, *Thin Solid Films* **2004**, *508*, 451–452.
[50] J. Nelson, *Phys. Rev. B* **2003**, *67*, 155209.
[51] We note we have previously referred to this energy offset as ΔG_{CS}^{eff}; several colleagues have pointed out to us that this energy offset is primarily an enthalpy rather than free energy difference.
[52] We note that this observation would be consistent with a model whereby charge separation proceeds primarily to relative amorphous PCBM, whilst charge collection, and cell voltage, is primarly determined by the (higher) EA of the aggregated domains, consistent with the lower cell voltages observed for PCBM relatively to ICBA. However further energetic studies, beyond the scope of this paper, will be necessary before this point can be addressed with confidence.
[53] C. F. Shen, A. Kahn, I. Hill, *Conjugated Polym. Mol. Interfaces* **2002**, 351.
[54] M. A. Faist, T. Kirchartz, W. Gong, R. S. Ashraf, I. McCulloch, J. C. de Mello, N. J. Ekins-Daukes, D. D. C. Bradley, J. Nelson, *J. Am. Chem. Soc.* **2012**, *134*, 685.
[55] Z. L. Guan, J. B. Kim, H. Wang, C. Jaye, D. A. Fischer, Y. L. Loo, A. Kahn, *Organ. Electron.* **2010**, *11*, 1779.
[56] J. M. Hodgkiss, A. R. Campbell, R. A. Marsh, A. Rao, S. Albert-Seifried, R. H. Friend, *Phys. Rev. Lett.* **2010**, *104*, 177701.
[57] A. C. Morteani, P. Sreearunothai, L. M. Herz, R. H. Friend, C. Silva, *Phys. Rev. Lett.* **2004**, *92*, 247402.
[58] S. K. Pal, T. Kesti, M. Maiti, F. Zhang, O. Inganas, S. Hellstrom, M. R. Andersson, F. Oswald, F. Langa, T. Osterman, T. Pascher, A. Yartsev, V. Sundstrom, *J. Am. Chem. Soc.* **2010**, *132*, 12440.
[59] D. Credgington, F. C. Jamieson, B. Walker, T.-Q. Nguyen, J. R. Durrant, *Adv. Mater.* **2012**, *24*, 2135.
[60] J. W. Zhou, B. R. Findley, C. L. Braun, N. Sutin, *J. Chem. Phys.* **2001**, *114*, 10448.
[61] J. Lee, K. Vandewal, S. R. Yost, M. E. Bahlke, L. Goris, M. A. Baldo, J. V. Manca, T. Van Voorhis, *J. Am. Chem. Soc.* **2010**, *132*, 11878.
[62] Y. Zhou, K. Tvingstedt, F. Zhang, C. Du, W.-X. Ni, M. R. Andersson, O. Inganas, *Adv. Funct. Mater.* **2009**, *19*, 3293.
[63] M. A. Faist, T. Kirchartz, J. Nelson, unpublished.
[64] Y. He, H.-Y. Chen, J. Hou, Y. Li, *J. Am. Chem. Soc.* **2010**, *132*, 1377.
[65] G. Zhao, Y. He, Y. Li, *Adv. Mater.* **2010**, *22*, 4355.
[66] C.-H. Cho, H. J. Kim, H. Kang, T. J. Shin, B. J. Kim, *J. Mater. Chem.* **2012**, *22*, 14236.
[67] R. D. Pensack, C. Guo, K. Vakhshouri, E. D. Gomez, J. B. Asbury, *J. Phys. Chem. C* **2012**, *116*, 4824.